

# Spectral Domain Polarization Sensitive Optical Coherence Tomography at 1.55 $\mu\text{m}$ : Novel Developments and Applications for Dynamic Studies in Materials Science

David Stifter\*<sup>a</sup>, Elisabeth Leiss-Holzinger<sup>b</sup>, Bettina Heise<sup>a,c</sup>, Jean-Luc Bouchot<sup>c</sup>, Zoltan Major<sup>d</sup>, Michael Pircher<sup>e</sup>, Erich Götzinger<sup>e</sup>, Bernhard Baumann<sup>e</sup>, Christoph K. Hitzenberger<sup>e</sup>

<sup>a</sup>Christian Doppler Laboratory for Microscopic and Spectroscopic Material Characterization, Center for Surface- and Nanoanalytics (ZONA), Johannes Kepler University Linz, Altenbergerstr. 69, 4040 Linz, Austria

<sup>b</sup>Research Center for Non Destructive Testing GmbH, Hafenstrasse 47-51, 4020 Linz, Austria

<sup>c</sup>Christian Doppler Laboratory for Microscopic and Spectroscopic Material Characterization, Department of Knowledge-Based Mathematical Systems (FLLL), Johannes Kepler University Linz, Altenbergerstr. 69, 4040 Linz, Austria

<sup>d</sup>Institute of Polymer Product Engineering, Johannes Kepler University Linz, Altenbergerstr. 69, 4040 Linz, Austria

<sup>e</sup>Center for Medical Physics and Biomedical Engineering, Medical University of Vienna, Währingerstr. 13, 1090 Vienna, Austria

## ABSTRACT

In this paper it is demonstrated, how research in optical coherence tomography (OCT) for biomedical diagnostics successfully triggered new developments in the field of mechanical material testing. With the help of a specifically designed, compact and robust spectral domain polarization sensitive OCT (SD-PS-OCT) setup, which is operating at 1.55  $\mu\text{m}$ , dynamic investigations of technical materials - like bulk polymers and composite samples - can be performed under various conditions. Already by evaluating the speckle pattern of the standard SD-OCT images with advanced image processing methods, valuable information on the deformation and flow characteristics of samples subjected to tensile tests can be obtained. By additionally taking the birefringence properties into account, complementary knowledge on the evolvement of the internal stress situation is obtained in a spatially resolved way.

**Keywords:** Polarization sensitive optical coherence tomography, birefringence imaging, speckle pattern evaluation, material characterization, mechanical testing

## 1. INTRODUCTION

Polarization sensitive optical coherence tomography (PS-OCT) was developed to provide additional contrast based on the birefringence properties of the samples under investigation [1,2]. Due to increased sensitivity of OCT in the Fourier domain (FD) with respect to conventional time domain (TD) imaging, PS-OCT was recently also implemented in the spectral domain configuration (SD-PS-OCT), mostly operating at a center wavelength of 800 nm [3] or to a smaller extent at 1300 nm [4].

Like the OCT method itself, PS-OCT is still nearly exclusively developed for and used in the field of biomedical diagnostics, although all OCT techniques provide promising potential for alternative applications [5], like in the field of material science and non-destructive testing. In the case of PS-OCT it was shown with systems operating in the TD, that information on the internal strain/stress distribution of scattering materials can be obtained in a spatially resolved way [6-12].

\*david.stifter@jku.at; phone +43 732 2468 8881; fax +43 732 2468 8843; www.jku.at/zona

Inspired from the findings of the biomedical diagnostics community, where data is rapidly acquired with FD-OCT for volumetric or dynamic imaging, we consequently realized a compact and robust SD-PS-OCT setup for the dynamic investigation of technical materials [13], like bulk polymers and composites under various loading conditions in mechanical testing, as presented in this paper. Since light absorption by water is no issue for these materials, our experiments are performed at an imaging wavelength of 1.55  $\mu\text{m}$  to provide increased penetration depth [5].

## 2. EXPERIMENTAL

The SD-PS-OCT setup is schematically depicted below in Figure 1. The setup is based on the concept described in [3], but uses a 1.55  $\mu\text{m}$  superluminescence diode as light source, which provides a depth resolution of  $\sim 13 \mu\text{m}$  in typical polymer materials (e.g.  $n \sim 1.45$ ). Furthermore, the free-space interferometer head is realized in a compact and robust way, so it can easily be integrated into e.g. state-of-the-art mechanical testing equipment. The sample itself is irradiated with circular polarized light (up to 2.5 mW) and the – in general – elliptical polarized light, which is back reflected from the sample, is combined with the linear polarized light coming from the reference arm (oriented at  $45^\circ$  with respect to the horizontal). The vertical and horizontal polarized components are then detected by two grating spectrometer units with 4kHz InGaAs line cameras (Sensors Unlimited, 1024 pixels). From the two polarization channels reflectivity, optical retardation and axis orientation images are simultaneously obtained [3] - with a sensitivity of 95 dB from the B-scan data (512 x 1024 pixels), which are acquired by raster scanning the focused light with the Galvano mirror over the sample (lateral resolution  $\sim 14 \mu\text{m}$ ).

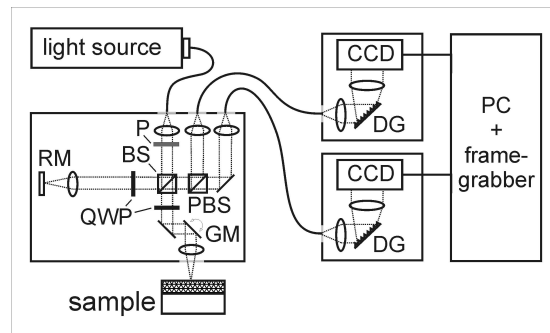


Figure 1. Schematic sketch of SD-PS-OCT setup, with: reference mirror (RM), polarizer (P), beamsplitter (BS), polarizing BS (PBS), quarter wave plates (QWP), galvano-scanner mirror (GM), diffraction gratings (DG), line cameras (CCD).

As samples for the demonstration of imaging during tensile testing, 1 mm thick shouldered test bars from elastomer particle filled polypropylene (PP) and from a polyurethane elastomer were prepared. In addition, glass fiber-reinforced epoxy sheets (pre-impregnated fiber composite materials), as used for the fabrication of helicopter rotor blades [10], were prepared for fracture tests.

## 3. RESULTS AND DISCUSSION

Since mechanical testing is routinely performed in a dynamic way, we show in the next sections the potential of SD-OCT and SD-PS-OCT to obtain valuable information derived from changes of the optical properties occurring in the interior of scattering samples.

### 3.1 SD-OCT imaging at 1550 nm for mechanical testing

For the development of new materials, mechanical testing is used to obtain parameters like elastic modulus, yield stress or flow stress with typical tensile testing machines. In the case of polymers, the introduction of elastomer particles in a rigid homopolymer matrix like PP is currently of high interest, in order to obtain materials with increased toughness and impact strength [14], as needed for applications in e.g. the automotive industry. In this context, digital image correlation

(DIC) [15] equipment is routinely applied in addition to the (global/overall) mechanical tests to locally study the deformation of the sample surface. To obtain information on the internal changes within such scattering samples, new optical methods like OCT and optical coherence elastography [16] are needed.

In the following we can show, that even for highly scattering materials subjected to large deformations, which lead to uncorrelated speckle patterns between subsequent frames, useful information can be obtained already from standard SD-OCT images by carefully evaluating the temporal statistical behavior and similarities of the speckle pattern. These speckle patterns are mainly caused due to the random distributed backscatterers within the polymer and are carrying material specific information. Especially moving speckles may indicate a flowing behavior of the material under test. Therefore, we propose to evaluate the dynamics of such spatially distributed and evolving flow fields comparing locally consecutive frames of OCT reflectivity images taken over time with respect to their statistical and local similarities. For our considerations, we apply a method which computes the local discrepancy between image regions, based on the work of Baudrier et al. [17]. While therein the authors introduced a so-called Local Dissimilarity (LD) map to compare binary images, here we are interested in an extraction of the LD map for gray scale data of random speckle patterns. The LD map can be defined as:

$$LD[d](I_k, I_{k+1})(i,j) = d(I_k \circ 1_{A_{i,j}}, I_{k+1} \circ 1_{A_{i,j}}),$$

where  $d$  represents a chosen (dis)similarity measure,  $I_k$  and  $I_{k+1}$  denote two temporally subsequent scans, and  $1_A$  describes the indicator function for a small local neighborhood at the location  $(i,j)$ . The computation of the LD gives valuable insights into the stretched polymer material containing both, locally flowing sample regions (e.g. plastically deforming regions where necking occurs) and locally remaining static regions.

Following the definition above, two main parameters are important to consider: the similarity measure  $d$  and the local window size  $n$ . First, we study the influence of the similarity measure. It is used to describe the local resemblance or dissimilarity between two overlapping regions in both frames. The measures based on statistics such as Bhattacharyya distance [18] or mutual information [19] only take the distribution of the pixel intensities into account. Therefore, they only allow estimating whether the distribution function of speckle patterns remains more or less constant over time regardless of incoming and outgoing speckles and their displacements. These measures seem appropriate for a single frame analysis but less suitable for comparing different frames. In contrast, we suggest applying pixel-based measures, since the spatial ordering of the pixels is important, although we are also aware of the influence of noise, which may hamper such pixel-based comparisons.

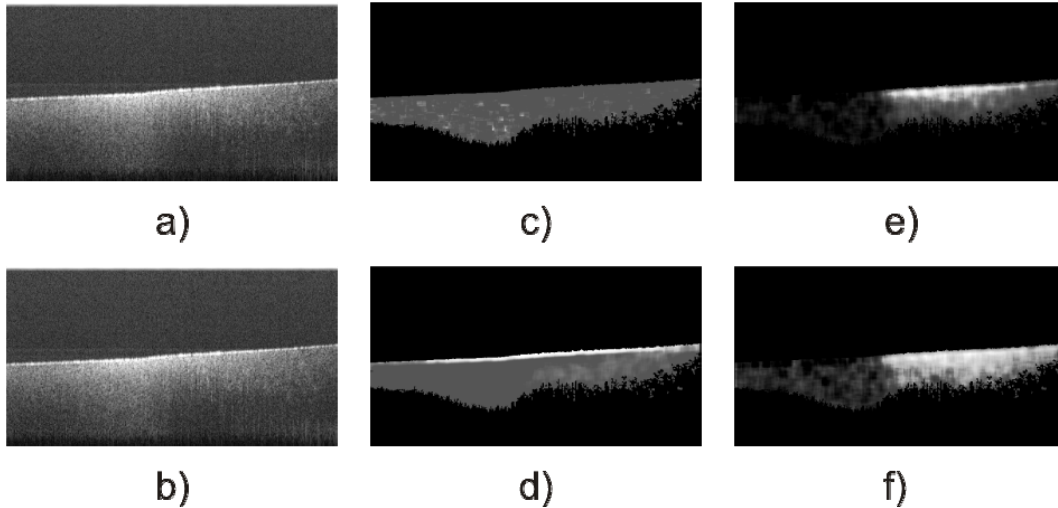


Figure 2. Dissimilarity characterization applying different similarity measures for local flow pattern analysis exemplified on a strained PP polymer sample: a) and b) two consecutive cross-sectional OCT reflectivity scans taken during tensile testing; the computed LD maps applying c) the Bhattacharyya distance, d) the mutual information, e) the  $L_1$ -norm, and f) the  $L_2$ -norm as similarity measures. The spatially differing behavior of the material under test and the front of flow can be clearly recognized. All the dissimilarity maps are calculated within a local neighborhood ( $n \times n$ ) with  $n=28$  pixels. Grayscale coding: The transition from an almost static to dynamic behavior is represented from white to dark gray and black, within a masked region of interest.

Figure 2 illustrates the influence of the choice of different measures for the resulting LD map. In particular, we have evaluated the dissimilarity by exploiting the Bhattacharyya distance and the mutual information as statistical measures, as well as by computing the  $L_1$ - and the  $L_2$ - norm (i.e. the sum of absolute values and the Euclidean norm) as pixel-based measures. According to our results for two subsequent frames, acquired during tensile testing and depicted in Figures 2 a) and b), the statistics-based measures are rather unreliable here, as shown in Figure 2 c) and d), although the static and flowing domains may be partly differentiated by the mutual orientation estimation (the sample boundary introduces a small artifact in the analysis). However, the classical  $L_p$ - norms obviously provide clearer results: the different regions are easily discernable, as illustrated in Figures 2 e) and f). In our representation the lighter shadings represent static regions, whereas darker regions express a stronger dynamics of the speckle pattern.

Furthermore, we find that the  $L_2$ - norm gives rather more consistent results than the  $L_1$ - norm, in the sense that the different sample regions are homogeneously separated and therefore the front of the material flow during tensile loading can be better recognized.

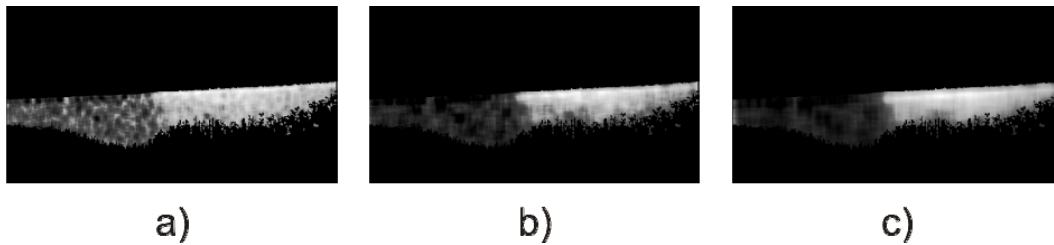


Figure 3. Dissimilarity characterization applying different window sizes for the local flow pattern analysis: the two consecutive cross-sectional OCT scans according to Figure 2 are used to compute the LD map within a local neighborhood window ( $n \times n$ ) with a)  $n= 16$ , b)  $n= 28$ , and c)  $n= 44$  pixels. As dissimilarity measure the  $L_2$ -norm is used.

As second parameter, we investigate the influence of the size of the local neighborhood on the resulting dissimilarity map. By varying the window size for calculating the LD maps, we can find that the results strongly depend on the size of the considered local neighborhood, as shown in Figure 3. Indeed, smaller regions will allow a better description of the flow, but the consistency/coherence of the individual regions is partly lost. In contrast, by using a larger neighborhood rather consistent regions are provided in the image, but at the cost of lower spatial accuracy. Consequently, a trade-off for our experimental application had to be made, yielding a window size of  $28 \times 28$  pixels for optimized results.

By repeating the similarity analysis at different deformation states during the tensile testing experiment, namely at the beginning of the plastic deformation, at an intermediate state of permanent plastic deformation, and immediately before the fracture of the material, comparative information is gained, as illustrated in Figure 4. In the early beginning of the stretching process, the material is still almost transparent. Only few small opaque particles may be observed in Figure 4 a) and b), which are slightly displaced by the sample straining, resulting for LD in a slightly darker central region in Figure 4 c). At an intermediate state the polymer is then becoming fully scattering, as can be seen in Figure 4 d) and e). In the corresponding LD map - depicted in Figure 4 f) - one clearly may distinguish two different regions: while the brighter region corresponds to an almost static part within the material, the black region hints at higher speckle dynamics caused by material flowing. Finally, the dissimilarity becomes strongest when the material reaches a point shortly before fracture, as shown in Figure 4 g) and h). It is evident from the LD map, that the underlying sample microstructures are strongly disturbed and entirely moving: the previously separated regions are getting merged, as can be observed from Figure 4 i).

Summarizing, although local flow pattern characterization shows potential to be refined by DIC methods, as used for the characterization of surface deformations, the above introduced similarity analysis methods already allow to effectively characterize material dynamics and to provide information on the distribution of flowing regions from simple SD-OCT images.

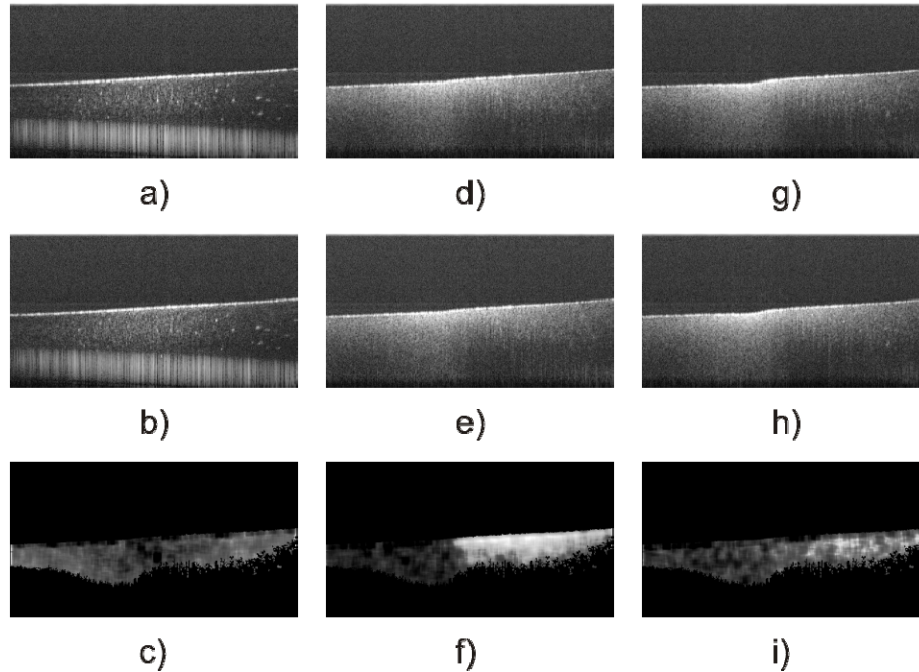


Figure 4. Dissimilarity characterization at different temporal states during the tensile test experiment: two subsequent cross-sectional OCT reflectivity scans are chosen a) and b) at the beginning of plastic deformation showing only a weakly scattering central region; d) and e) at an intermediate state with fully developed material scattering, and g) and h) directly before sample fracture. The corresponding LD maps are depicted in c), f), and i). As dissimilarity measure the  $L_2$ -norm is used with a window size of  $28 \times 28$  pixels.

### 3.2 Birefringence imaging with SD-PS-OCT at 1550 nm for mechanical testing

In a complementary way to the above findings from SD-OCT imaging and by taking advantages of the strain/stress-birefringence response of the polymer samples, SD-PS-OCT gives access to the internal strain/stress distribution. This has been already shown in detail for samples under quasi-static loading conditions with TD-PS-OCT [6-12]. With the SD-PS-OCT technique recordings can now simultaneously be made to dynamic mechanical tests, shedding light on the internal stress evolution. As depicted in Figure 5, retardation cross section scans of scattering polymer samples (in this case a polyurethane elastomer material with a thickness of up to 1 mm) with a distinct fringe pattern are obtained during a typical tensile test with strain rates of  $\sim 1$  mm/s. These velocities pose no problem for dynamic SD-PS-OCT imaging. Furthermore, the influence of mechanical creep and stress relaxation, as routinely observed for such polymers under quasi-static loading conditions – needed for slow TD-PS-OCT imaging – is thus minimized during the acquisition of a single frame.

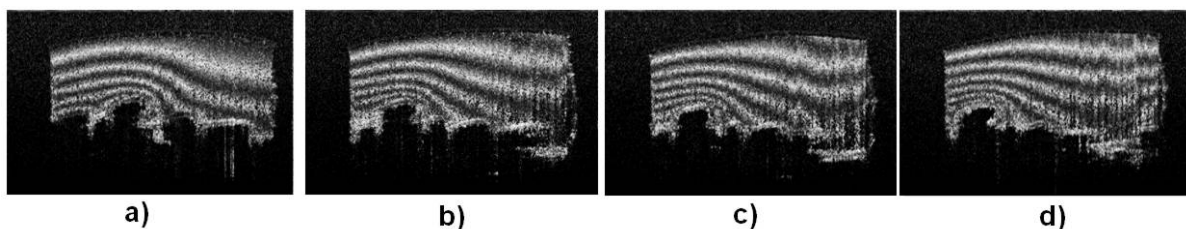


Figure 5. Retardation images of a scattering polyurethane elastomer polymer sample (average thickness  $\sim 1$ mm) with increasing load (a-d) in a dynamic tensile test.

The retardation images, as depicted in Figure 5, are grey scale encoded with phase increments of  $\pi/2$  between successive black and white stripes. Thus, a high spatial frequency of the fringe structures corresponds to increased values of birefringence and consequently strain/stress. With the help of advanced mathematical analysis of retardation fringe structures, as introduced at first in [12] on TD-PS-OCT data, 2D birefringence and stress maps can be obtained, as exemplified in Figure 6 for one retardation cross section.

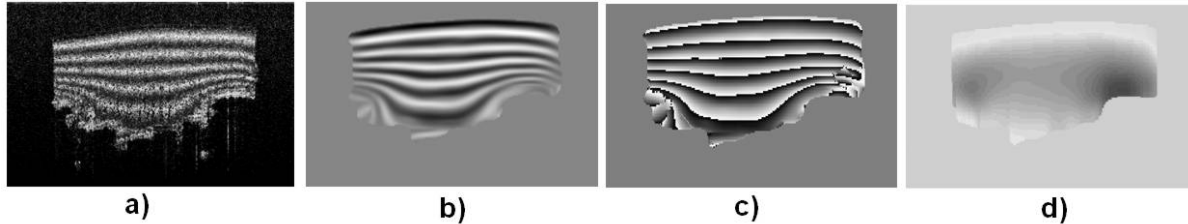


Figure 6. 2D demodulation procedure and image processing: a) original retardation image of the strained polymer sample, b) image after coherence enhancing diffusion denoising, c) wrapped phase image via 2D radial Hilbert transform, d) image after unwrapping and taking the derivate (normalized birefringence/stress image).

With respect to the required 2D demodulation procedure of the phase retardation images [12,13], we want to provide the following additional considerations: although simple stripe patterns observed in typical tensile testing can be in principle efficiently processed by one-dimensional demodulation methods of the individual A-scans, a 2D analysis - as depicted in Figure 6 - offers the advantage of exploiting the full 2D spatial frequency information encoded in the fringe pattern. In particular, the possibility to combine fringe image demodulation methods based on the 2D radial Hilbert transform [20] or on the Riesz transform [21] with an appropriate image denoising techniques, as e. g. coherence enhancing diffusion (CED) methods [22], allows the complete geometrical analysis of the retardation B-scans. In addition, if a slowly varying background is present in the images, superimposed on the fringe pattern, the application of a 2D Empirical Mode Decomposition (EMD) method [23] is recommended by us for a locally non-zero mean background correction. As it is demonstrated in Figure 7, the pattern in the bottom region of the retardation images, where lower fringe visibility prevails due to decreased signal-to-noise-ratio, is better resolved with this further developed 2D demodulation approach: especially for complex geometries, like the one observed and magnified in the insets of Figure 7, an improvement in the continuation of the fringe structures is clearly obtained.

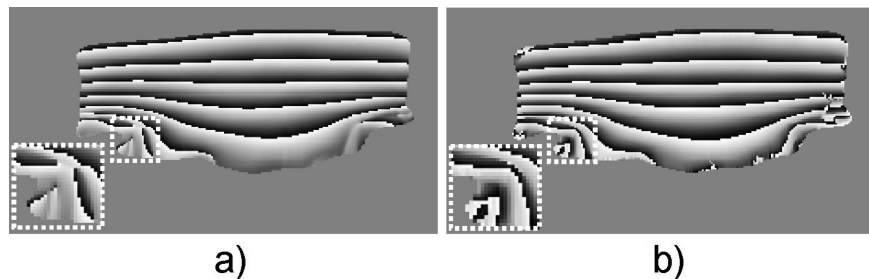


Figure 7. Wrapped phase images calculated from a cross-sectional retardation image without (a) and with (b) EMD correction prior demodulation with 2D Hilbert Transform (insets with enlarged views of marked regions).

As a final example for this work, the application of SD-PS-OCT for a time resolved study of damage formation in glass fiber composites (GFC) during fracture tests is presented. In the case of Figure 8, the sample was bent over a rigid edge, till complete structural failure occurs, with debris flying off the sample (corresponding spots marked in the right reflectivity image). In contrast to the findings obtained in [10] under quasi-static loading conditions, the sequence of reflectivity and retardation images of Figure 8 allows to study the temporal evolvement of defects like delaminations between fiber structure and matrix (as e.g. indicated by the arrow in the middle reflectivity image), occurring in regions

of increased stress, as determined from the simultaneously obtained retardation images (marked region in middle retardation image).

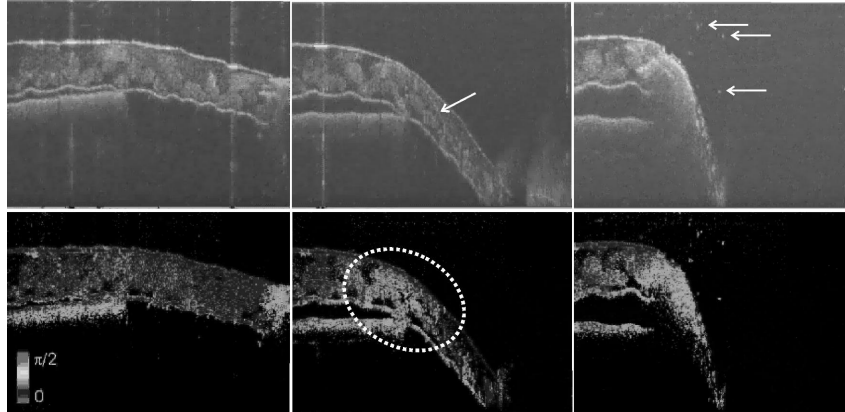


Figure 8. Sequence of reflectivity (top row) and retardation (bottom row) cross sections taken with SD-PS-OCT from a glass fiber composite sheet during fracture.

#### 4. CONCLUSIONS AND OUTLOOK

Summarizing, we have shown that SD-PS-OCT - originally developed for biomedical imaging and now performed at  $1.55\ \mu\text{m}$  in conjunction with mechanical testing – has the potential to provide essential new insights for experimental mechanics and into the performance/characteristics of technical materials in a time and spatially resolved way. The fact that structural details and polarization characteristics can simultaneously be obtained from the inside of scattering materials demonstrates the superior characteristics of SD-PS-OCT over conventional optical techniques, like e.g. standard transmission photoelasticity methods or DIC.

With respect to future work, we would like to guide the focus on the improvement of the spatial resolution for resolving technical details (like micrometer sized single fibers or filler particles), by either employing novel widely tunable swept sources or broadband sources for the  $1.5\ \mu\text{m}$  region: preliminary tests by us with supercontinuum sources driven by compact nanosecond pulse lasers or by femtosecond fiber lasers are currently underway and have shown that the axial resolution can easily be improved by more than a factor of two.

#### ACKNOWLEDGEMENTS

The financial support by the Austrian Science Fund (project P19751-N20), the European Regional Development Fund in the framework of the EU-programme Regio 13, the federal state Upper Austria, the Federal Ministry of Economy, Family and Youth and the National Foundation for Research, Technology and Development is gratefully acknowledged.

#### REFERENCES

- [1] M. R. Hee, D. Huang, E. A. Swanson, and J. G. Fujimoto, "Polarization-sensitive low-coherence reflectometer for birefringence characterization and ranging," *J. Opt. Soc. Am. B-Opt. Phys.* 9, 903-908 (1992).
- [2] J. F. de Boer, T. E. Milner, M. J. C. van Gemert, and J. S. Nelson, "Two-dimensional birefringence imaging in biological tissue by polarization sensitive optical coherence tomography," *Opt. Lett.* 22, 934-936 (1997).
- [3] E. Götzinger, M. Pircher, and C. K. Hitzenberger, "High speed spectral domain polarization sensitive optical coherence tomography of the human retina," *Opt. Express* 13, 10217-10229 (2005).
- [4] B.H. Park, M.C. Pierce, B. Cense, S.H. Yun, M. Mujat, G.J. Tearney, B.E. Bouma, and J.F. de Boer, "Real-time fiber-based multi-functional spectraldomain optical coherence tomography at  $1.3\ \mu\text{m}$ ," *Opt. Express* 13, 3931-3944 (2005).

- [5] D. Stifter, "Beyond biomedicine: a review of alternative applications and developments for optical coherence tomography," *Appl. Phys. B* 88, 337-357 (2007).
- [6] D. Stifter, P. Burgholzer, O. Höglinger, E. Götzinger, and C. K. Hitzenberger, "Polarisation-sensitive optical coherence tomography for material characterisation and strain-field mapping," *Appl. Phys. A* 76, 947-951 (2003).
- [7] J.-T. Oh and S.-W. Kim, "Polarization-sensitive optical coherence tomography for photoelasticity testing of glass/epoxy composites," *Opt. Express* 11, 1669-1676 (2003).
- [8] K. Wiesauer, A. D. Sanchis Dufau, E. Götzinger, M. Pircher, C. K. Hitzenberger, and D. Stifter, "Non-destructive quantification of internal stress in polymer materials by polarisation sensitive optical coherence tomography," *Acta Materialia* 53, 2785-2791 (2005).
- [9] K. Wiesauer, M. Pircher, E. Götzinger, C.K. Hitzenberger, R. Engelke, G. Ahrens, G. Grützner, and D. Stifter, "Transversal ultrahigh-resolution polarization-sensitive optical coherence tomography for strain mapping in materials," *Opt. Express* 14, 5945-5953 (2006).
- [10] K. Wiesauer, M. Pircher, E. Götzinger, C.K. Hitzenberger, R. Oster, and D. Stifter, "Investigation of glass-fibre reinforced polymers by polarization-sensitive, ultra-high resolution optical coherence tomography: internal structures, defects and stress," *Comp. Sci. Techn.* 67, 3051-3058 (2007).
- [11] J.S. Chen, and Y.K Huang, "Full-field mapping of stress-induced birefringence using a polarized low coherence interference microscope," *Proc. SPIE* 7133, 7133I-1 (2009).
- [12] B. Heise, K. Wiesauer, E. Götzinger, M. Pircher, C.K. Hitzenberger, R. Engelke, G. Ahrens, G. Grützner and D. Stifter, "Spatially resolved stress measurements in materials with polarization-sensitive optical coherence tomography: image acquisition and processing aspects," *Strain* 46, 61-68 (2010).
- [13] D. Stifter, E. Leiss-Holzinger, Z. Major, B. Baumann, M. Pircher, E. Götzinger, C.K. Hitzenberger, B. Heise, „Dynamic optical studies in materials testing with spectral-domain polarization-sensitive optical coherence tomography”, *Opt. Express* 18, 25712-25725 (2010).
- [14] P. A. Tzaika, M. C. Boyce, and D. M. Parks, "Micromechanics of deformation in particle toughened Polyamides," *J. Mech. Phys. Solids* 48, 1893–1929 (2000).
- [15] M. A. Sutton, J. J. Orteu, and H. Schreie, [Image Correlation for Shape, Motion and Deformation Measurements Basic Concepts, Theory and Applications], Springer, 2009.
- [16] J. M. Schmitt, "OCT elastography: imaging microscopic deformation and strain of tissue," *Opt. Express* 3(6), 199–211 (1998).
- [17] E. Baudrier, F. Nicolier, G. Millon and S. Ruan, "Binary-image comparison with local-dissimilarity quantification," *Pattern Recognition* 41, 1461-1478 (2008).
- [18] A. Bhattacharyya, "On a measure of divergence between two statistical population defined by probability distribution," *Bull. Calcuta Math.* 35, 99-109 (1943).
- [19] A. Papoulis, [Probability, Random Variables, and Stochastic Processes], McGraw-Hill, Inc., 3<sup>rd</sup> Ed. (1991).
- [20] K. G. Larkin, D. J. Bone, and M. A. Oldfield, "Natural demodulation of two-dimensional fringe patterns. I. General background of the spiral phase quadrature transform," *J. Opt. Soc. Am. A* 18, 1862-1870 (2001).
- [21] T. Bülow, D. Pallek, and G. Sommer, "Riesz Transforms for the Isotropic Estimation of the Local Phase of Moiré Interferograms," in [Mustererkennung], ed. G. Sommer et al., Springer (2000).
- [22] J. Weickert, "Coherence-enhancing diffusion filtering," *Int. J. Comput. Vision* 31, 111- 127 (1999).
- [23] C. Damerval, S. Mignen, V. Perrier, "A Fast Algorithm for Bidimensional EMD," *IEEE Sign. Proc. Lett.* 12, 701-704 (2005).